Composite Structures 271 (2021) 114164

Contents lists available at ScienceDirect

Composite Structures

journal homepage: www.elsevier.com/locate/compstruct

Crashworthiness design of periodic cellular structures using topology optimization

Jiao Jia [a], Daicong Da [b], Jianxing Hu [c], Sha Yin [c,*]

[a] Flying College, Beihang University, Beijing 100191, China
[b] Department of Mechanical Engineering, Northwestern University, Evanston, IL 60208, USA
[c] Vehicle Energy & Safety Laboratory (VESL), Department of Automotive Engineering, School of Transportation Science & Engineering, Beihang University, Beijing 100191, China

ARTICLE INFO

Keywords:
Crashworthiness design
Topology optimization
Cellular structure
Hybrid cellular automata (HCA)

ABSTRACT

Periodic cellular structures are widely used in structural protection due to their lightweight and excellent energy absorption characteristics, but the corresponding crashworthy design is still limited. Based on the framework of hybrid cellular automata (HCA), the optimal design of periodic cellular structure for crashworthiness is carried out. To guarantee the periodicity of cellular structure, elemental internal energy (EIE) is redistributed averagely as a periodic constraint. Then, by iteratively modifying the local EIE target, the cellular structure is optimized until the maximum energy absorption (EA) is obtained under the specific volume fraction constraint. Through several 2D and 3D numerical examples, this design method is proved to be efficient for the crashworthiness design of periodic cellular structures. Specifically, EA of the optimized cellular structures in this study can be improved by design comparing with solid structures and classical honeycombs. Effects of cellular number and volume gradient on crashworthiness are also discussed.

1. Introduction

Crashworthiness is highly demanded in high-end equipment from various industries, e.g., automotive, transportation and aerospace [1]. Periodic cellular structure has attracted wide attention as excellent lightweight energy absorbers for crashworthiness applications [2,3]. The deformation mode and energy absorption (EA) of cellular structures depend on the topology of unit cell. Ruan et al. [4] investigated the hexagonal honeycomb and discussed effects of cell wall thickness on the localized deformation modes. Also, three in-plane deformation modes (i.e., X mode, V mode and I mode) were discovered respectively corresponding to low, moderate and high impact velocities. Other honeycombs, e.g., square [5,6], triangle [7,8] are also widely applied in EA. Square and triangular honeycombs absorb energy through plastic yielding of side walls, while hexagonal honeycomb depends on the plastic hinges at the apex possessing a relatively stable deformation mode. With the rapid development of additive manufacturing (AM) technology, lots of periodic cellular structures were feasible to fabricate, e.g., lattice structure, hierarchical structure, gradient structure. These new structures could bear more complicated loads with higher specific energy absorption (SEA). McKown et al. [9] and Ozdemir et al. [10] experimentally studied EA characteristics of body-centred cubic (BCC) and diamond structures, respectively. Hu et al [11] explored the impact mitigation of double helical metamaterials inspired by the DNA structure. Hybrid structure combines the advantages of different cellular structures to obtain a better structural performance [12,13]. The hybrid of lattice truss and square honeycomb, named as honeytube, is superior to its constitutive structures from the perspective of SEA [14]. Similar strategy by structural hybrids had also been employed in Refs [15,16]. Nature's materials, e.g., butterfly wing, cancellous bone, often exhibit remarkable mechanical properties with additional structure hierarchy. Initially proposed by Lakes [17], hierarchical cellular structure had recently received extensive attention in EA applications. Qiao and Chen [18] proposed a hexagonal hierarchical structure, whose cell walls are composed of triangular honeycombs, and investigated the mechanical behavior under quasi-static and dynamic loads. Inspired by pomelo peel, a novel hierarchical structure is constructed with higher SEA [19]. Also, experimental results indicated that the mechanical properties of self-similar hierarchical octet-truss lattice structures were irrelevant to the relative density, but determined by the strut slenderness ratios in the two hierarchical levels [20]. Regarding on gradient cellular structures, Shen et al. [21] designed a hexagonal honeycomb whose deformation modes were observed different as impact loading

* Corresponding author.
E-mail address: shayin@buaa.edu.cn (S. Yin).

https://doi.org/10.1016/j.compstruct.2021.114164
Received 29 December 2020; Revised 21 April 2021; Accepted 21 May 2021
Available online 24 May 2021

on the weaker or stronger end. Assembled by the BCC unit cell, the gradient structure exhibited superior EA than the uniform structure [22]. Although various periodic cellular structures had been proposed, most of them were empirically designed or directly inspired by nature materials, and a systematic design method is still limited.

As an effective lightweight design tool, structural topology optimization had developed several popular approaches, e.g., solid isotropic material with penalization (SIMP) method [23–25], bi-directional evolutionary structural optimization (BESO) method [26,27], level set method (LSM) [28,29], moving morphable components (MMC) [30,31]. These algorithms were all typically sensitivity-based. However, sensitivities could not be easily obtained when the problem involved geometry, material and contact nonlinearity simultaneously, and thus limited research had been focused on the crashworthiness optimization. Huang et al. [32] used two criterions to deduce the discretized sensitivities of crashworthiness optimization based on BESO. In addition, equivalent static load (ESL) method [33] was proved to be efficient by replacing the complicated nonlinear dynamic problem with the simple linear elastic optimization one. As a non-sensitivity topology optimization technology, hybrid cellular automata (HCA) was popular in crashworthiness design. Panel et al. [34] successfully introduced the HCA into the crashworthiness optimization. In HCA, the design domain was discretized by cellular automata (CA) cells, and the physical quantities (e.g., elemental internal energy (EIE)) were updated by following the full-stressed principal. By dividing the design domain into flexible and rigid areas, Bandi et al. [35] proposed an energy-controlled strategy, where the flexible area was used to absorb energy versus the rigid area played a supporting role. Duddeck et al. [36] developed an optimization methodology for crashworthiness of thin-walled structures combining the ground structure approach and HCA. The local plastic hinge lines occurred because lots of shell elements were used to simulate the thin walls. Accordingly, HCA could fast iterate and converge, which was easy for secondary development with no requirement of sensitivity.

This study focuses on extending HCA for the crashworthiness design of periodic cellular structures and is organized as followed. The optimization methodology for crashworthy cellular structure is described in detail in Section 2. Then, in Section 3, the superiority of the optimized cellular structures, governing factors of the optimization results and model adaption in 3D problem are discussed through several numerical examples.

2. Optimization methodology

As illustrated in Fig. 1, one beam, composed of $m_x \times m_y$ periodic cellular cells, is subjected to an impact loading under the prescribed boundary conditions. Where m_x and m_y are the cellular numbers along x and y directions, respectively. The whole structure is further divided into $m \times n$ CA cells which are overlapped with the finite element (FE) meshes, where n is the number of finite elements in each cellular cell. In each CA cell, two field variables are defined, i.e., EIE $U_{i,j}$ and elemental relative density $x_{i,j}$, where i and j stand for cellular and CA cell labels, respectively. Note that the cellular structure corresponds to a solid crashworthy structure as $m = 1$.

Generally, EA of metal structure depends on plastic deformation and folding [34], which can be calculated by the enclosed curved area of external force and its corresponding structural deformation. Alternatively, for a structure discretized by the finite elements, EA can be represented by $\sum_{i=1}^{M}\sum_{j=1}^{N} U_{i,j}$ as well, indicating that more energy needs to be stored in elements to improve the EA capacity of structure. As illustrated in Fig. 2, energy in each element generally includes two parts, i.e., elastic energy $U_{i,j}^{e}$ and plastic energy $U_{i,j}^{p}$. However, $U_{i,j}^{e}$ should not be considered in the final EA owing to its recoverability.

Following the full-stress principal, HCA adopts a local control strategy to achieve the global optimization. The algorithm will retain the element whose EIE is greater than the target value, and delete the ones whose EIE is smaller than the target value, so as to maximize the EA capacity under the specific volume fraction constraint. In the optimization, $x_{i,j}$ is the design variable and the final topology can be generated by optimizing $x_{i,j}$ to 0 or 1.

Based on the above description, the crashworthiness optimization of periodic cellular structure can be formulated as

$$\begin{cases} \text{find} & x_{i,j} \\ \min & \|\hat{\tilde{U}}_{i,j} - U^{*}\| & (1.1) \\ \text{s.t.} & \boldsymbol{M}\ddot{\boldsymbol{s}} + \boldsymbol{C}\dot{\boldsymbol{s}} + \boldsymbol{K}\boldsymbol{s} = \boldsymbol{F} & (1.2) \\ & \sum_{i=1}^{m}\sum_{j=1}^{n} x_{i,j} V_{i,j} = V_f^{*} & (1.3) \\ & x_{\min} \leqslant x_{i,j} \leqslant 1 & (1.4) \\ & x_{1,j} = x_{i,j} \ldots = x_{m,j} & (1.5) \end{cases}$$

Different with other optimization formulation, Eq. (1.1) is an expression of locally operating on the EIE to evolutionarily achieve the global target. Where $\hat{\tilde{U}}_{i,j}$ is the effective EIE, and its solution will be detailed stated in Section 2.2. U^{*} is the target EIE which should be decided according to the specific requirement. In Eq. (1.2), $\boldsymbol{M}$, $\boldsymbol{C}$ and $\boldsymbol{K}$ are mass, damping and stiffness matrices, respectively. $\ddot{\boldsymbol{s}}$, $\dot{\boldsymbol{s}}$ and $\boldsymbol{s}$ respectively represent acceleration, velocity and displacement. Solving Eq. (1.2) is relatively slow because impact is a complicated dynamic problem involving geometry, material and contact nonlinearity, simultaneously. Generally, two schemes can be selected to solve crash problems, i.e., explicit and implicit schemes. Compared with the implicit scheme, the explicit scheme has superiority in computational time and convergence. Due to the nonlinear solver needs to be

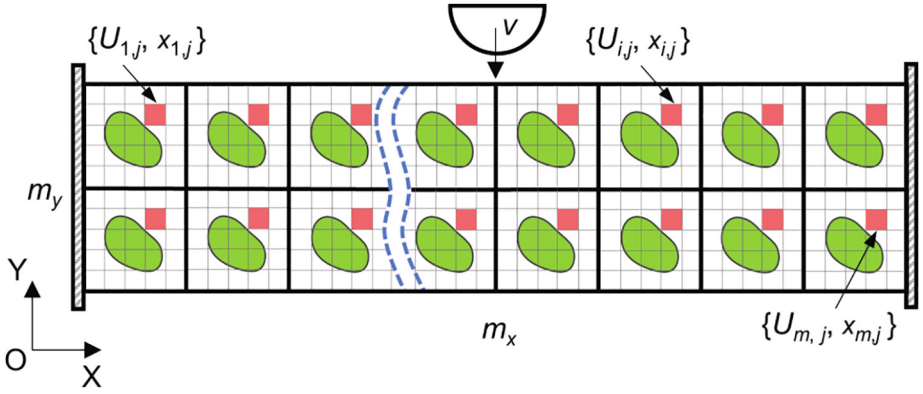

Fig. 1. Crashworthiness optimization of periodic cellular structure with HCA method.

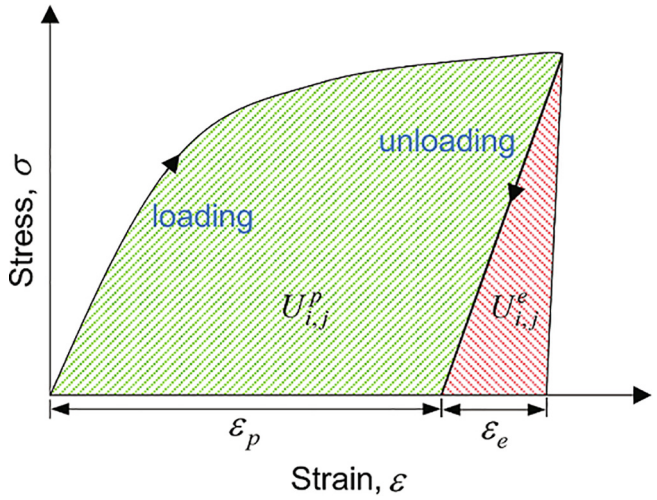

Fig. 2. Composition of energy at the element level. Notes: $U^p_{i,j}$ and $U^e_{i,j}$ stand for plastic energy and elastic energy, respectively.

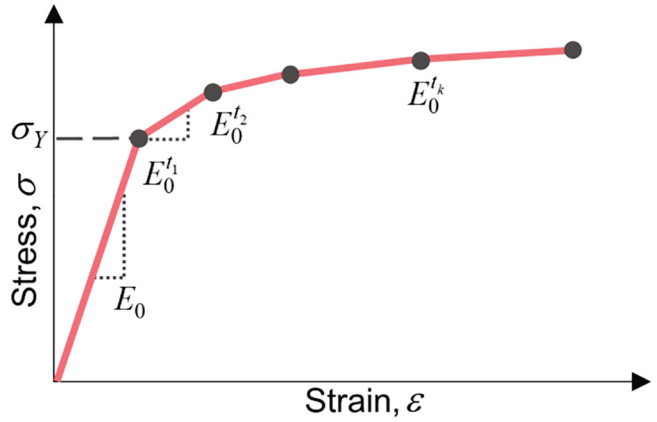

Fig. 3. A piecewise linear model with describing the elastic–plastic material behavior.

iteratively used in the optimization, the explicit scheme is adopted in this article. Eq. (1.3) confines the dosages of materials to be equal to V_f^*, where $V_{i,j}$ is the jth elemental volume in cellular cell i. In Eq. (1.4), to avoid the possible singularity, $x_{\min}$ is set to be 0.05 instead of 0.001 in linear optimization, because smaller $x_{\min}$ will affect the efficiency of FE solution when the problem involves nonlinearity. With the evolution of structural topologies, excessive low-density elements still cause the convergence problem. To alleviate this artificial stiffness problem, the elements will be removed from the FE model if $x_{i,j} \leqslant x_{\min}$. Although the elements are deleted, the design variables still exist in CA cells with a value of 0.05. And the deleted ones will be allowed to return to the FE model once $x_{i,j} > x_{\min}$ again. In order to satisfy the periodicity of cellular structures, Eq. (1.5) denotes the status of design variables at the same position in different cellular cells.

2.1. Material interpolation

Due to impact is always accompanied by the plastic deformation, only the elastic assumption is no longer applicable. And the plastic behavior of the material should be considered as well. As illustrated in Fig. 3, a piecewise linear model is constructed to approximately describe the elastic–plastic behavior in each element, as

$$E_{i,j} = x_{i,j}^p E_0 \tag{2.1}$$

$$\sigma_{i,j}^Y = x_{i,j}^p \sigma_0^Y \tag{2.2}$$

$$E_{i,j}^{t_k} = x_{i,j}^p E_0^{t_k} \tag{2.3}$$

where E_0, σ_0^Y, $E_0^{t_k}$ are Young's modulus, yield stress, hardening modulus of the base material. It can be seen from Eqs. (2.2) and (2.3) that the stress will vary with the design variable $x_{i,j}$ when plastic deformation happens. p is a penalization parameter whose value is set as 1 [34].

Meanwhile, the elemental material density also varies with the design variable $x_{i,j}$ as

$$\rho_{i,j} = x_{i,j}\rho_0 \tag{3}$$

where ρ_0 is the density of the base material.

2.2. Updating rules and convergence criteria

Without sensitivity information, the update of design variable $x_{i,j}$ mainly depends on the deviation between the target value and the effective EIE. In this work, the proportional control strategy is adopted to restrain the amplitude change of $x_{i,j}$.

$$x_{ij}^{(l+1)} = x_{ij}^{(l)} + \Delta x_{ij}^{(l)} \tag{4}$$

$l\Delta x_{ij}^{(l)}$

$$\Delta x_{ij}^{(l)} = \max\{-0.1, \min\{C_p(\tilde{\tilde{U}}_{i,j}^{(l)} / U^{*(l)} - 1), 0.1\}\} \tag{5}$$

where C_p is the proportional gain to control the amplitude change of $x_{i,j}$. The suggested value of C_p is 0.2 according to the numerical tests. More-

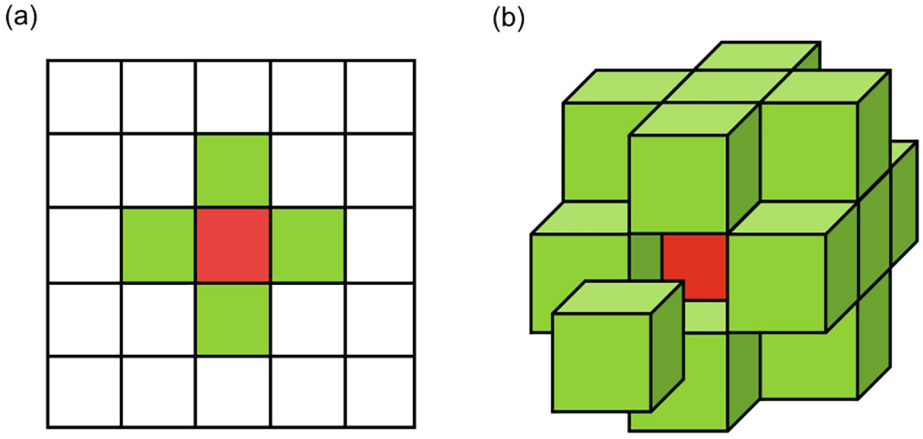

Fig. 4. CA neighborhood layouts: (a) 2D Von Neumann $ne = 4$; (b) 3D radial $ne = 18$.

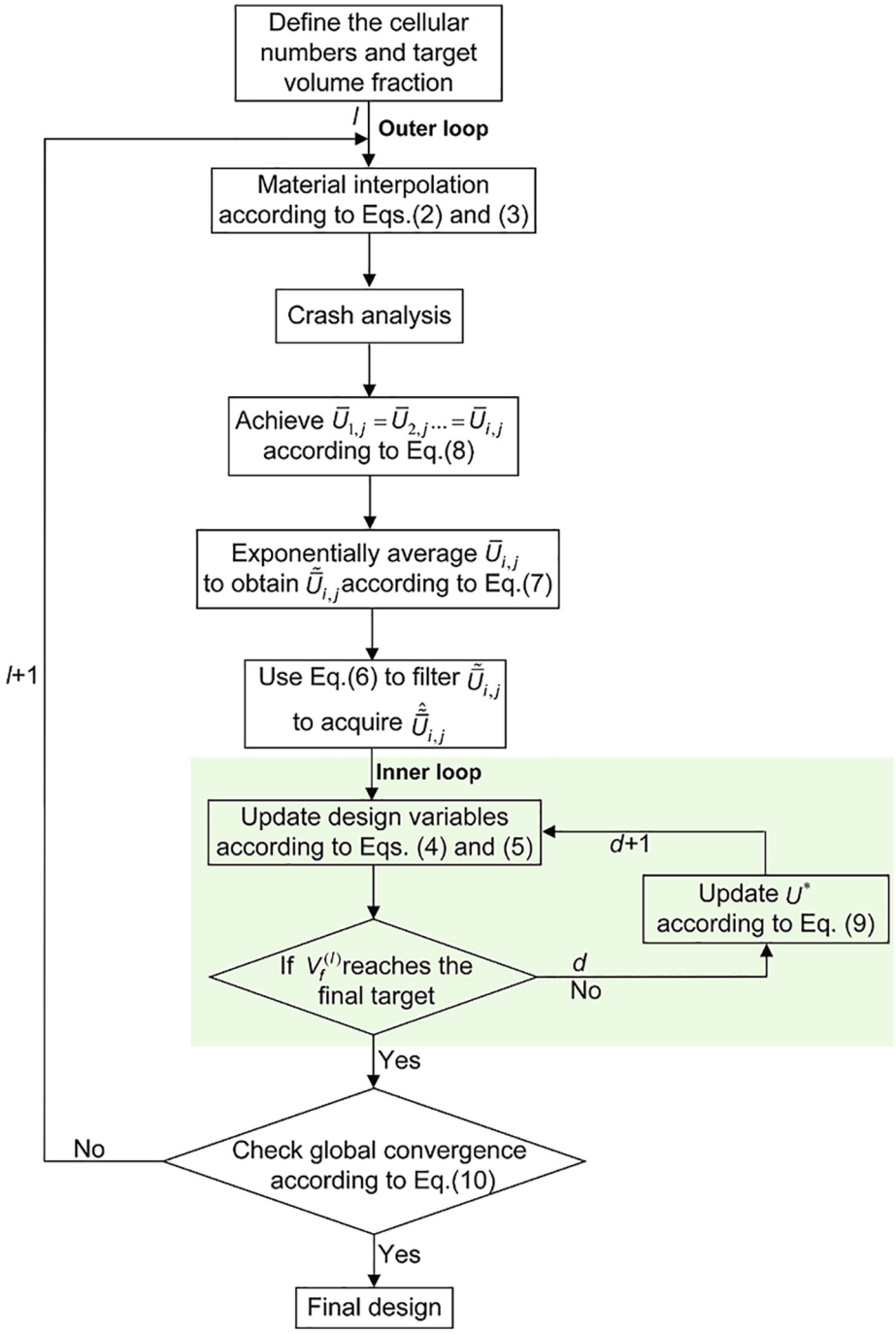

Fig. 5. Flow chart of crashworthiness topology optimization of periodic cellular structure.

Table 1
Material parameters of aluminum [34].

Property	Value
Density (kg/m^3)	2700
Elastic modulus (GPa)	70
Yield stress (MPa)	180
Strain hardening (/MPa)	(0.00, 180), (0.01, 190) (0.02, 197), (0.05, 211.5) (0.1, 225.8), (0.15, 233.6) (0.2, 238.5), (0.4, 248.5)

over, a maximum move limit of 0.1 is enforced on $\Delta x_{i,j}$ to avoid the iterative instability in the optimization. The effective EIE $\hat{\tilde{\bar{U}}}_{i,j}$ is mutually decided by the values of CA cell j and its neighborhood. Using an averaging strategy, the effective $\hat{\tilde{\bar{U}}}_{i,j}$ can be obtained through

$$\hat{\tilde{\bar{U}}}_{i,j} = \frac{\tilde{\bar{U}}_{i,j} + \sum_{e=1}^{ne} \tilde{\bar{U}}_{i,e}}{ne + 1} \tag{6}$$

where $\tilde{\bar{U}}_{i,j}$ and $\tilde{\bar{U}}_{i,e}$ respectively represent the averaged EIE in CA cell j and its neighboring CA cells with considering the historical information. ne is the total number of CA cells in the neighborhood. In Fig. 4, red and green blocks stand for the CA cell j and its neighborhood. The von Neumann layout including 4 neighbors and the radial layout including 18 neighbors are adopted in 2D design and 3D design, respec-

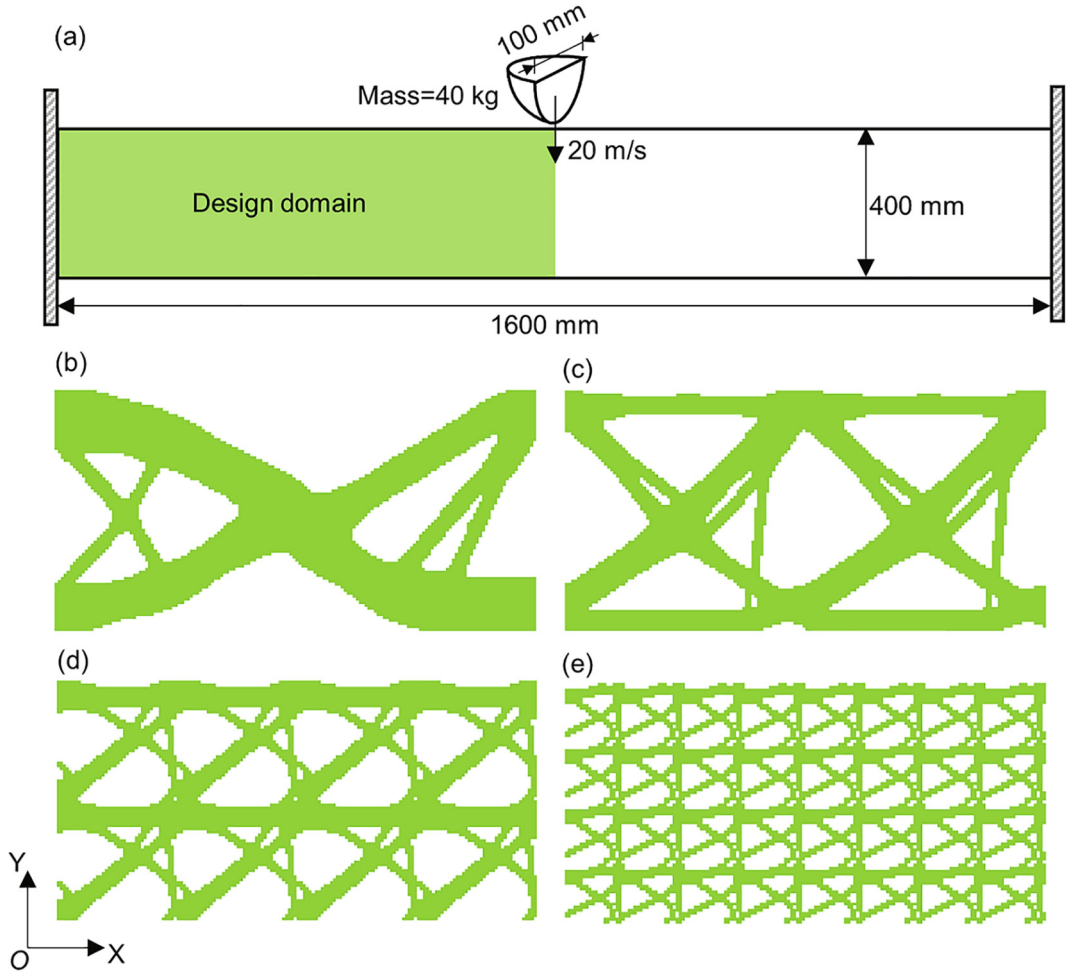

Fig. 6. Schematic information of 2D fully-clamped beam and resulting half-span topologies: (a) design domain and boundary conditions; (b) solid structure; cellular structure with $m_x \times m_y$ (c) = 2 × 1; (d) = 4 × 2; (e) = 8 × 4.

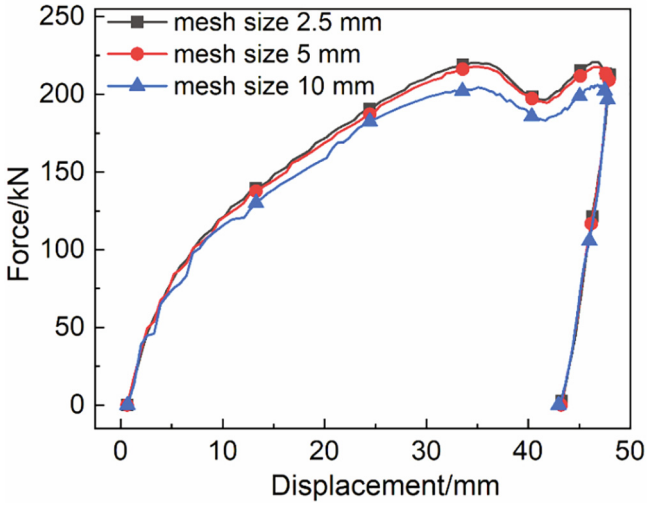

Fig. 7. The force–displacement curves of the initial structure with different mesh sizes.

tively. Actually, this average strategy can be viewed as the filter in SIMP, which can prevent the checkerboard and mesh dependency phenomena in the optimization.

In the optimization, material distributions usually oscillate between the iterations due to the instability of solving dynamic problems. This problem can be substantially relieved through averaging the EIE with its historical information. Therefore, $\tilde{U}_{ij}$ in Eq. (6) can be written as

$$\tilde{U}_{ij}^{(l)} = \frac{1}{\sum_{q=0}^{3} w_{ij}^{q}} \sum_{q=0}^{3} w_{ij}^{q} \bar{U}_{ij}^{(l-q)} \tag{7}$$

where w_{ij} is the weight factor and can be written as $(x_{ij} - x_{\min})^2$. Three previous information of EIE is utilized in this work.

The periodic cellular structure can be realized when $x_{1j} = x_{ij} \ldots = x_{mj}$. From Eqs. (4)–(7), it is easily known that if $\bar{U}_{1j} = \bar{U}_{ij} \ldots = \bar{U}_{mj}$, we will have $x_{1j} = x_{ij} \ldots = x_{mj}$ finally. In order to satisfy the above relationship, $\bar{U}_{ij}$ can be averaged as

$$\bar{U}_{1j} = \bar{U}_{ij} \ldots = \bar{U}_{mj} = \sum_{i=1}^{m} U_{ij}/m \tag{8}$$

where U_{ij} is the actual EIE value directly obtained by FE solver. Although Eq. (8) is simple, it keeps the internal energy of the whole structure constant during EIE redistribution process. Note that although FE solving is enforced on the whole structure, the update process of x_{ij} can be conducted only in a representative unit cell to save computational cost because of the periodicity.

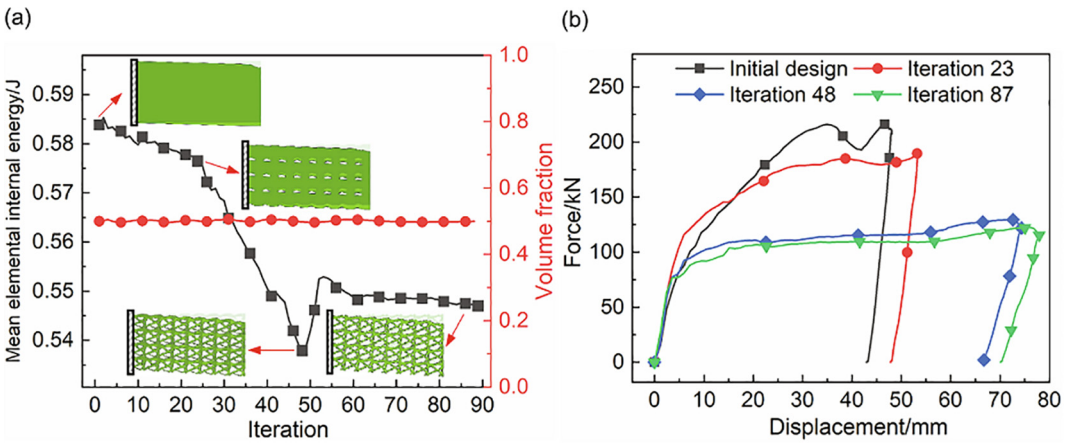

Fig. 8. Iteration of cellular structure with $m_x \times m_y = 8 \times 4$: (a) iterative histories of mean EIE and volume fraction constraint; (b) force–displacement curves of different iterative steps.

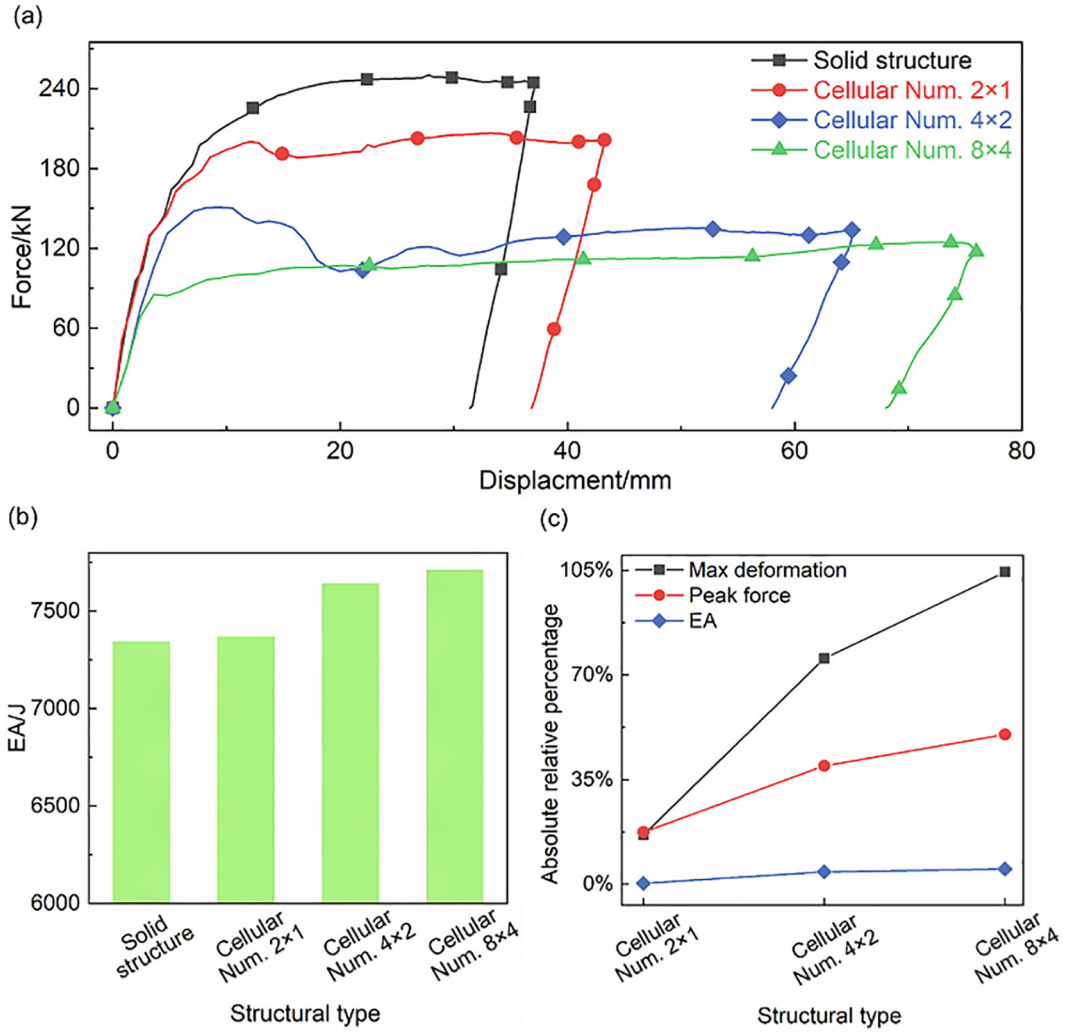

Fig. 9. Crashworthiness performance with different cellular numbers: (a) force–displacement curves; (b) EA capacity; (c) sensitivities of cellular numbers versus crashworthiness indicators.

An inverse relationship exists between the target EIE and target volume fraction, serving as the foundation of the volume constraint. Furthermore, in order to restrain the actual volume fraction as the target one, a secondary inner iteration is adopted. In the sub-loop, the target EIE is constantly updated according to

$$U^{*(d+1)} = U^{*(d)}(V_f^{(d)}/V_f^*) \tag{9}$$

where $V_f^{(d)}$ is the material volume fraction in the dth sub-loop step. The sub-loop will stop when $|V_f^{(d)} - V_f^*| \leqslant 0.5\%$.

The optimization iteration will terminate when

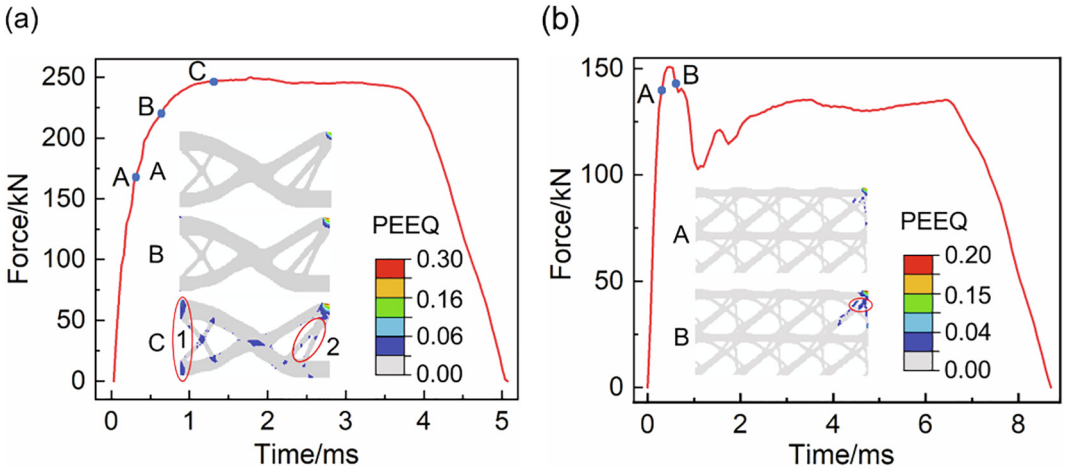

Fig. 10. Equivalent plastic strain–time plot of different type of structures:(a) solid structure; (b) cellular structure with $m_x \times m_y = 4 \times 2$.

Fig. 11. Resulting cellular structure in consideration of orthotropic constraint.

$$\frac{|\Delta V^{(l)}| + |\Delta V^{(l-1)}|}{2V_0} \leqslant \varepsilon \tag{10}$$

where V_0 stands for the volume of full design. The change of volume between two adjacent iteration steps ΔV can be expressed as $V^{(l)} - V^{(l-1)}$, where $V^{(l)}$ and $V^{(l-1)}$ respectively decide the material volume in lth and (l - 1)th iteration steps. Based on trial testing, the convergence tolerance ε is set as 0.1% in the current work.

The key steps for the crashworthiness topology optimization of periodic cellular structures are given in Fig. 5.

3. Numerical examples

In this section, effects of cellular number, volume gradient, and model adaption in the 3D design are discussed in detail through several numerical examples. Although this work is to maximize the capacity of EA, initial peak force and maximum deformation [1] are also discussed to overall evaluate the crashworthiness of optimized cellular structures. In all the numerical examples, the beams are designed to be impacted by rigid poles under different boundary conditions. The rigid pole is modeled with discrete rigid shell elements. A reference point with concentrated mass is built on the rigid pole. Moreover, the degrees of the reference point in x and z directions are constrained and an initial velocity in -y direction is enforced. In 2D examples, the design domains are discretized by shell elements with constraining out-plane freedom for easily enforcing self-contacts. During the impact, two contacts are considered, i.e., the contact between the rigid pole and the beam, the self-contact of the beam. The friction coefficient between the pole and the beam is assumed as 0.3 [35]. In the current study, aluminum metallic material is adopted, whose specific property is given in Table. 1. In the optimization, the initial design starts from the intermediate density with the value of target volume fraction, i.e., $x_{ij} = V_f^*$. The optimization algorithm is programmed in Matlab in integration with nonlinear FEA solver, such as Abaqus.

3.1. 2D problems

3.1.1. Example I: A fully-clamped beam

The effect of cellular number is investigated with $m = m_x \times m_y = 1 \times 1$, 2×1,4×2 and 8×4. As illustrated in Fig. 6 (a), the half model with enforcing the symmetric boundary conditions is adopted in the optimization for improving the computational efficiency, which is adopted in the following examples. In this example, the target volume fraction V_f^* is set as 50%, and the beam is subjected to impact loading with a 40 kg rigid pole and an initial velocity of 20 m/s. The design domain is discreted by mesh size of 5 mm × 5 mm with a thickness of 20 mm. The mesh dependence analysis of the initial structure is shown in Fig. 7, and good convergence could be observed when mesh size is 5 mm. In consideration of the computational efficiency, the mesh size of 5 mm is selected in the following 2D examples. From Fig. 6(b-e), the optimized cellular structures are significantly different with m. Meanwhile, all the topological figures present anisotropic, which reflects the impact loading direction very well. If not specified in the article, EA is adopted instead of SEA because the mass keeps the same.

3.1.1.1. Robustness of the proposed method. In Fig. 8(a), it can be observed that the volume fraction can satisfy the target value very well. Mean EIE overall declines, although some oscillations exist during the iteration. According to several representative topologies from the initial design to the converged result, it can be observed that the deformation of the beam is localized at the initial, and then tends to deform integrally as the topology evolves. The beam becomes softer when iteration increases, accompanied by larger structural deformation and lower peak force as shown in Fig. 8(b).

3.1.1.2. Effects of cellular number on crashworthiness. In Fig. 9(a), the solid structure and cellular structure with $m_x \times m_y = 8 \times 4$ have no apparent initial peak force. Therefore, the peak force is taken as the crashworthiness indicator in this example. For quantitative comparisons, EA of different structures are calculated according to Fig. 9(a), and shown in Fig. 9(b). Obviously, cellular structures have higher EA capacity and lower peak force. This is mainly due to that the material in solid structure presents a concentrated distribution versus an evenly distribution in cellular structure, which leads to cellular struc-

ture possessing lower peak force and larger structural deformation, and thus more energy is absorbed. Furthermore, with increasing of m from 2×1 to 8×4, the capacity of EA and maximum deformation monotonically increase by 4.7% and 75.4%, while the peak force monotonically drops by 39.6%. This indicates that the cellular number m is a key factor for crashworthiness of cellular structure, which will provide design guidance for its engineering application. Taking the solid structure as the benchmark, the absolute relative percentages of the crashworthiness indicators ($|(\mathrm{Inc} - \mathrm{Inc_s})/\mathrm{Inc_s}| \times 100\%$, where Inc and $\mathrm{Inc_s}$ are crashworthiness indicators of cellular structures and solid structure, respectively) can well reflect their sensitivities versus to cellular numbers m as shown in Fig. 9(c). It can be obtained that the maximum deformation is the most sensitive to cellular numbers, followed by the peak force and EA.

To explain that some optimized structures do not have the initial peak force, the deformation modes of solid structure and cellular structure with $m_x \times m_y = 4 \times 2$ are analyzed. At time points A and B, the solid structure deforms at the impacted end as shown in Fig. 10(a), versus the beam integrally bends around the restrained end (red circled region with 1) at time point C. Moreover, the local support structure (red circled region with 2) hardly involves the deformation during this period, so that a drop in load curve does not happen finally. However, in Fig. 10(b), tiny structural branches (red circled region) yield plastic deformation at the time point B and deduce a local unstability region, resulting in a sudden drop in load curve.

Table 2
Crashworthiness comparisons of cellular structures with and without orthotropic constraint.

Orthotropic constraint	EA (J)	Initial peak force (kN)	Max deformation (mm)
Yes	7722.7	120.0	76.4
No	7644.6	150.9	65.3

3.1.1.3. Effects of orthotropic constraint on crashworthiness. As averaging $\bar{U}_{ij}$ along the vertical and horizontal axes within a representative cellular after Eq. (8), the final topologies exhibit orthotropy. As an illustration, the cellular structure with $m_x \times m_y = 4 \times 2$ is optimized under the orthotropic constraint. As shown in Fig. 11, the optimized topological configuration is totally different with the resulting topology in Fig. 6(d). Through the quantitative comparisons in Table 2, as the material is more evenly distributed under the orthotropy constraint, a drop in peak force and an increase in max deformation happen. Correspondingly, the capacity of EA has a slight improvement.

3.1.2. Example 2: fixed-end beam

The influence of volume gradient is discussed in this example. In Fig. 12(a), the beam is impacted by a rigid pole with a mass of 50 kg at an initial velocity of 15 m/s. Cellular numbers along x and y axes are fixed as 9 and 3. Two gradient structures are investigated, i.e., from top to bottom, the volume fraction successively increases or decreases between 40% and 60% with a step of 10%. For comparison the resulting solid structure and uniform cellular structure under the equivalent volume constraint of 50% are also illustrated in Fig. 12 (b–c). From Fig. 12(c–e), it can be observed that the volume gradient has obvious influence on the resulting topologies of cellular structures.

3.1.2.1. Effects of volume gradient on crashworthiness design. As shown in Fig. 13(a-b), the solid structure has the lowest EA capacity, the highest initial peak force and the smallest structural deformation among the four structures. When compared with the uniform cellular structure, the cellular structures with volume gradient have no superiority in EA. However, their stiffness superiority can be demonstrated with the initial peak force increasing 21.4% and 33.5%, and the maximum structural deformation decreasing 19.9% and 19.5%. It is because that the materials excessively concentrate on the top and bottom of the beam to satisfy the volume gradient requirement, resulting in the gra-

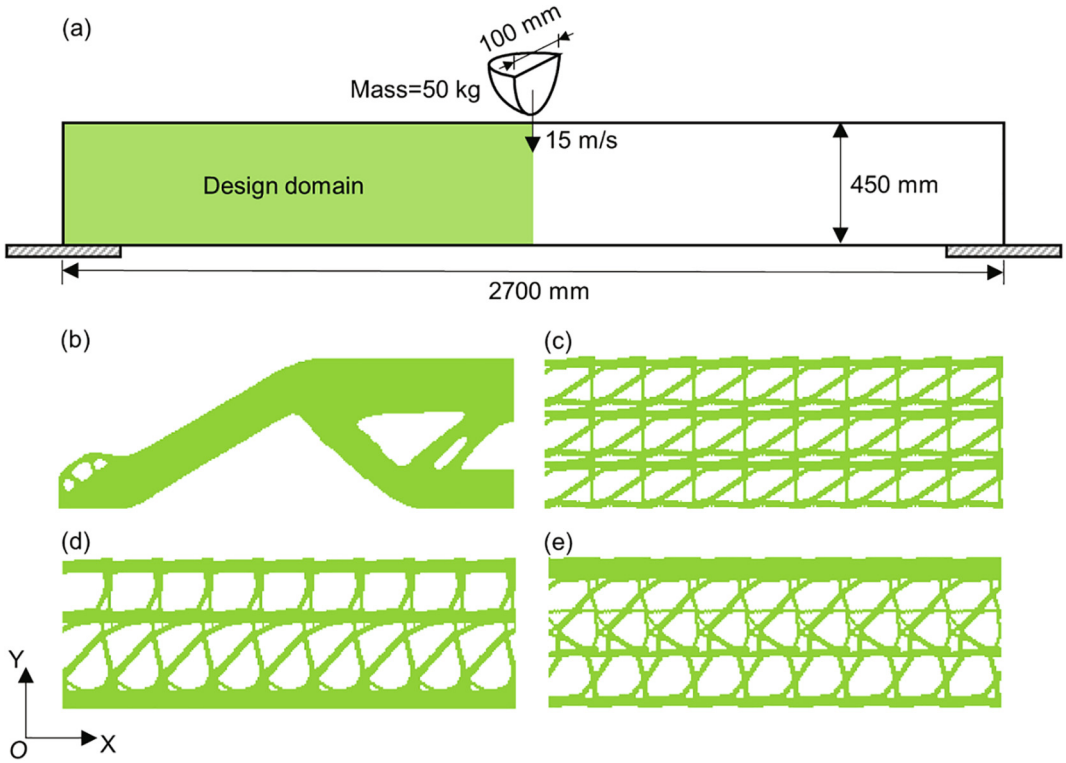

Fig. 12. Schematic information of 2D fixed-end beam and resulting half-span topologies: (a) design domain and boundary conditions; (b) solid structure; (c) uniform cellular structure; cellular structure with (d) increased volume gradient; (e) decreased volume gradient.

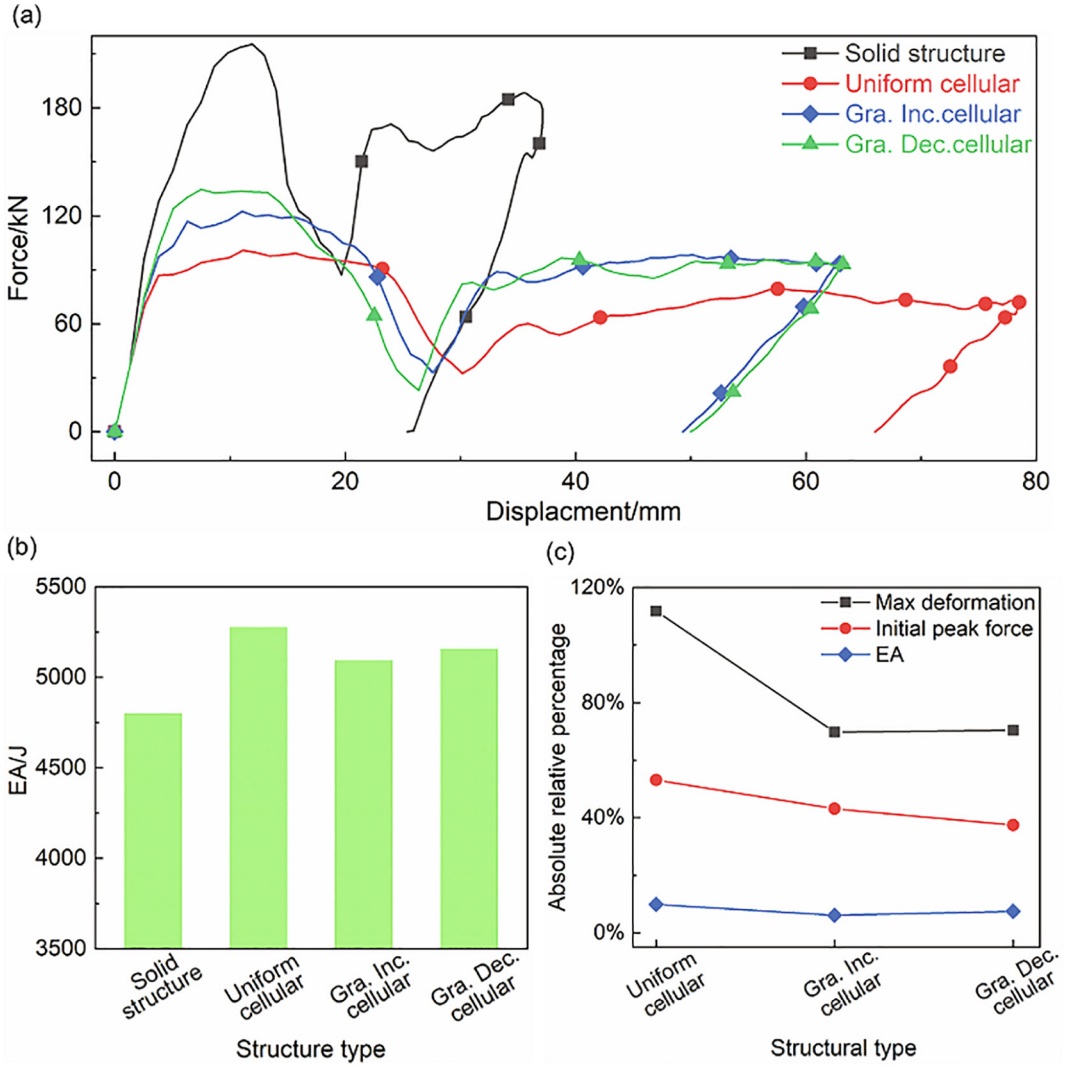

Fig. 13. Crashworthiness performance of different types of structures: (a) force–displacement curves; (b) EA capacity; (c) sensitivities of gradient on crashworthiness indicators.

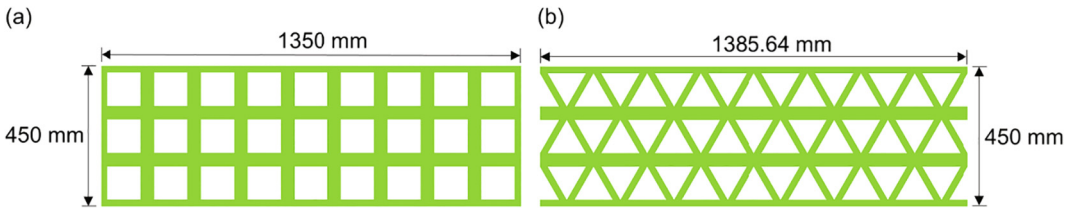

Fig. 14. Classical cellular structures for EA: (a) square cellular; (b) triangular cellular.

Table 3
Crashworthiness comparisons between the optimized and classical cellular structures.

Type of cellular structure	SEA (J/g)	Initial peak force (kN)	Max deformation (mm)
Optimized	0.3217	100.9	78.6
Square	0.3171	92.0	98.3
Triangular	0.3198	83.7	88.5

dient structure is stiffer than the uniform structure. Moreover, the cellular structure with decreased volume gradient has a higher initial peak force than the one with the increased volume gradient owing to a stiffer top. As illustrated in Fig. 13(c), the influences of volume gradient on crashworthiness indicators are in sequence of max deformation > initial peak force > EA capacity. Additionally, increasing or decreasing volume gradient from top to bottom only has a certain influence on the initial peak force, but litter influence on the max deformation and EA capacity.

3.1.2.2. Comparison with competing cellular structures. As shown in Fig. 14, the optimized uniform cellular structure is compared with the classical square and triangle honeycombs for illustrating the superiority of the proposed methodology. The feature mesh size of square and triangular honeycombs is limited to 5 mm as well. In Table 3, we

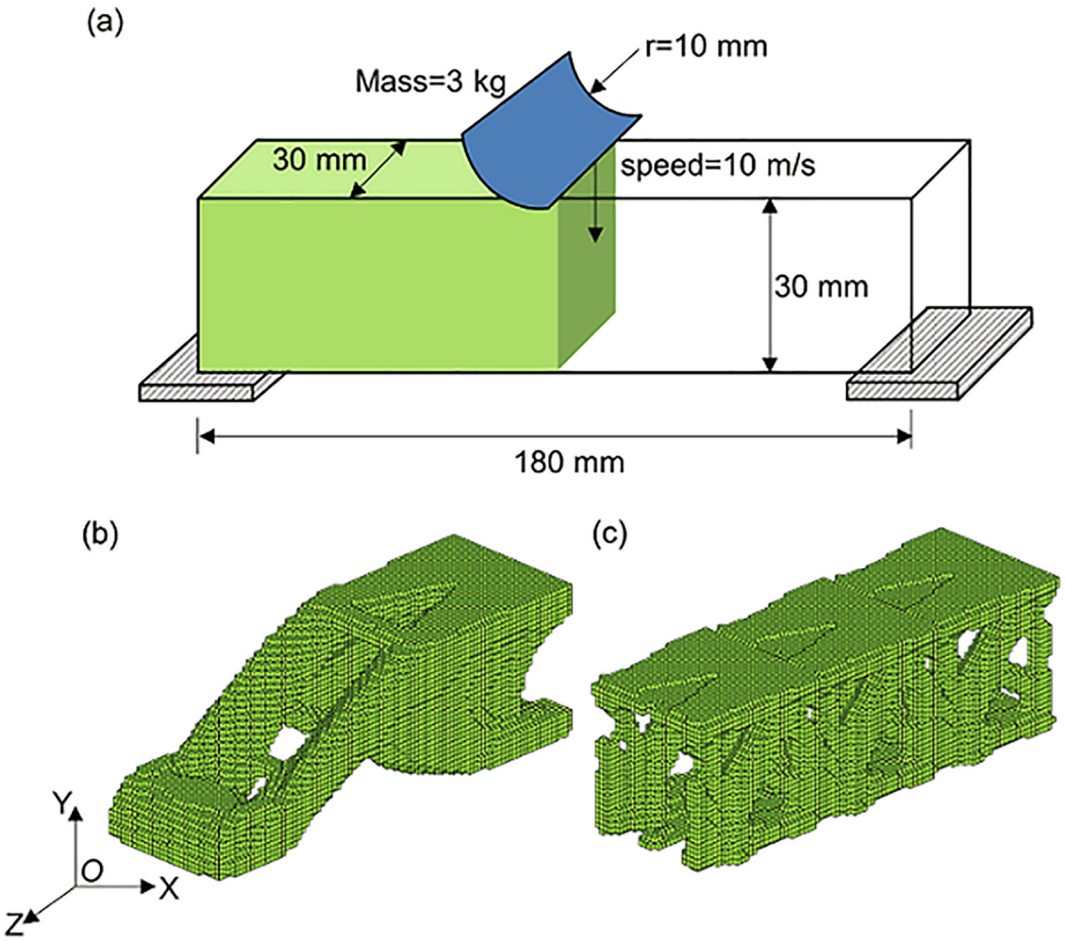

Fig. 15. Schematic information of 3D beam and resulting half-span topologies: (a) design domain and boundary conditions; (b) solid structure; (c) cellular structure with $m_x \times m_y = 3 \times 1$.

Table 4
Crashworthiness comparisons of solid structure and cellular structure with $m_x \times m_y = 3 \times 1$.

Type of structure	EA (J)	Initial peak force (kN)	Max deformation (mm)
Solid structure	121.0	13.1	11.7
Cellular structure with $m_x \times m_y = 3 \times 1$	131.3	8.4	18.5

select SEA instead of EA because that the triangular structure is heavier (16.8 kg) than the optimized structure (16.4 kg). Table 3 shows that the optimized cellular structure has the highest SEA capacity with the value of 0.3217 J/g. Compared with the square and triangular honeycombs, the initial peak force of the optimized structure respectively increases 9.7% and 20.5%. Meanwhile, the max deformation respectively decreases by 20% and 11.2%. These indicate that the optimized cellular structure has superior EA and stiffness performance. The above comparisons demonstrate that the current proposed method is effective in the crashworthiness design of cellular structures.

3.2. 3D numerical example

The adaption of 3D design is discussed in this section. As illustrated in Fig. 15(a), the rigid pole is 3 kg with an initial impact velocity of 10 m/s. The volume fraction constraint is set as 30%. Cellular numbers m_x and m_y are set as 3 and 1, respectively. The beam is discretized using 1 mm × 1 mm × 1 mm brick elements. Similarly, the resulting topology of the solid structure is demonstrated as well for comparison. As shown in Fig. 15(b-c), it can be observed that the optimized cellular structure is quite different with the solid structure. Similar to the 2D cases, the anisotropic topological configuration reflects the direction of the impact loading well. From Table 4, the optimized 3D cellular structure increases by 8.5% and 58.1% in EA capacity and structural deformation, and reduces by 35.9% in initial peak force with comparison of the solid structure. Finally, these results indicate that the proposed method can solve the 3D crashworthy optimization problem very well.

4. Conclusions

A topology optimization method for crashworthiness design of periodic cellular structures is developed in this study. Reallocating EIE as an additional constraint is employed to ensure the periodicity in the optimization iteration. The following conclusions are summarized as:

1) The optimized cellular structures possess higher EA capacity than the solid crashworthy structures and square/triangular honeycombs.
2) The EA capacity and maximum deformation increase while the initial peak force decreases with cellular number increasing. The maximum deformation is the most sensitive while the EA capacity is the least to the cellular number.

3) Compared with the uniform cellular structure, the gradient cellular structures possess superior stiffness but not EA. Also, effects of the volume gradient on max deformation and initial peak force are more significant than those on EA.
4) The proposed method can be extended to optimize the 3D periodic cellular structures.

Declaration of Competing Interest

The authors declare that they have no known competing financial interests or personal relationships that could have appeared to influence the work reported in this paper.

Acknowledgements

This work was financially supported by the Natural Science Foundation of China (NSFC) (No. 11902015).

References

[1] Lu G, Yu TX. Energy absorption of structures and materials. Woodhead Publishing; 2003.
[2] Evans AG, Hutchinson JW, Fleck NA, Ashby MF, Wadley HNG. The topological design of multifunctional cellular metals. Prog Mater Sci 2001;46(3-4):309–27.
[3] Gibson L, Ashby M. Cellular solids – Structures and properties. Cambridge University Press; 1997.
[4] Ruan D, Lu G, Wang B, Yu TX. In-plane dynamic crushing of honeycombs - a finite element study. Int J Impact Eng 2003;28(2):161–82.
[5] Xue Z, Hutchinson JW. Crush dynamics of square honeycomb sandwich cores. Int J Numerical Methods Eng 2006;65(13):2221–45.
[6] Becker JHB. Effective elastic properties of hexagonal and quadrilateral grid structures;1999.
[7] Liu Y, Zhang X-C. The influence of cell micro-topology on the in-plane dynamic crushing of honeycombs. Int J Impact Eng 2009;36(1):98–109.
[8] Hohe J, Becker W. Effective elastic properties of triangular grid structures. 1999;45 (2):131–45.
[9] McKown S, Shen Y, Brookes WK, Sutcliffe CJ, Cantwell WJ, Langdon GS, et al. The quasi-static and blast loading response of lattice structures. Int J Impact Eng 2008;35(8):795–810.
[10] Ozdemir Z, Hernandez-Nava E, Tyas A, Warren JA, Fay SD, Goodall R, et al. Energy absorption in lattice structures in dynamics: Experiments. Int J Impact Eng 2016;89:49–61.
[11] Hu J, Yu TX, Yin S, Xu J. Low-speed impact mitigation of recoverable DNA-inspired double helical metamaterials. Int J Mech Sci 2019;161-162:105050. https://doi.org/10.1016/j.ijmecsci.2019.105050.
[12] Ashby MF, Bréchet YJM. Designing hybrid materials. Acta Mater 2003;51 (19):5801–21.
[13] Fleck NA, Deshpande VS, Ashby MF. Micro-architectured materials: past, present and future. Proc R Soc A-Math Phys 2010;466(2121):2495–516.
[14] Yin S, Li J, Liu B, Meng K, Huan Y, Nutt SR, et al. Honeytubes: Hollow lattice truss reinforced honeycombs for crushing protection. Compos Struct 2017;160:1147–54.
[15] Ha CS, Lakes RS, Plesha ME. Design, fabrication, and analysis of lattice exhibiting energy absorption via snap-through behavior. Mater Des 2018;141:426–37.
[16] Harris JA, Winter RE, McShane GJ. Impact response of additively manufactured metallic hybrid lattice materials. Int J Impact Eng 2017;104:177–91.
[17] Lakes R. Materials with structural hierarchy. Nature 1993;361(6412):511–5.
[18] Qiao J, Chen C. In-plane crushing of a hierarchical honeycomb. Int J Solids Struct 2016;85-86:57–66.
[19] Zhang W, Yin S, Yu TX, Xu J. Crushing resistance and energy absorption of pomelo peel inspired hierarchical honeycomb. Int J Impact Eng 2019;125:163–72.
[20] Sha Y, Jiani Li, Haoyu C, Ritchie RO, Jun Xu. Design and strengthening mechanisms in hierarchical architected materials processed using additive manufacturing. Int J Mech Sci 2018;149:150–63.
[21] Shen CJ, Lu G, Yu TX. Dynamic behavior of graded honeycombs - A finite element study. Compos Struct 2013;98:282–93.
[22] Maskery I, Hussey A, Panesar A, Aremu A, Tuck C, Ashcroft I, et al. An investigation into reinforced and functionally graded lattice structures. J Cell Plast 2017;53(2):151–65.
[23] Bendsøe MP. Optimal shape design as a material distribution problem. Struct Optimiz 1989;1(4):193–202.
[24] Sigmund O, Maute K. Topology optimization approaches A comparative review. Struct Multidiscip Optimiz 2013;48(6):1031–55.
[25] Chen Z, Long K, Wen P, Nouman S. Fatigue-resistance topology optimization of continuum structure by penalizing the cumulative fatigue damage. Adv Eng Softw 2020;150:102924. https://doi.org/10.1016/j.advengsoft.2020.102924.
[26] Querin OM, Young V, Steven GP, Xie YM. Computational efficiency and validation of bi-directional evolutionary structural optimisation. Comput Methods Appl Mech Eng 2000;189(2):559–73.
[27] Li Yu, Xie YM. Evolutionary topology optimization for structures made of multiple materials with different properties in tension and compression. Compos Struct 2021;259:113497. https://doi.org/10.1016/j.compstruct.2020.113497.
[28] Wang MY, Wang X, Guo D. A level set method for structural topology optimization. Comput Meth Appl Mech Eng 2003;192(1-2):227–46.
[29] Wei P, Wang W, Yang Y, Wang MY. Level set band method: A combination of density-based and level set methods for the topology optimization of continuums. Front Mech Eng-Prc 2020;15(3):390–405.
[30] Guo X, Zhang WS, Zhong WL. Doing Topology Optimization Explicitly and Geometrically-A New Moving Morphable Components Based Framework. J Appl Mech 2014;81(8):081009.
[31] Liu C, Du Z, Zhu Y, Zhang W, Zhang X, Guo Xu. Optimal design of shell-graded-infill structures by a hybrid MMC-MMV approach. Comput Methods Appl Mech Eng 2020;369:113187. https://doi.org/10.1016/j.cma.2020.113187.
[32] Huang X, Xie YM, Lu G. Topology optimization of energy-absorbing structures. Int J Crashworthines 2007;12(6):663–75.
[33] Park G-J. Technical overview of the equivalent static loads method for non-linear static response structural optimization. Struct Multidiscip Optimiz 2011;43 (3):319–37.
[34] Patel NM, Kang BS, Renaud JE, Tovar A. Crashworthiness design using topology optimization. J Mech Des 2009;131(6):061013.
[35] Bandi P, Schmiedeler JP, Tovar A. Design of crashworthy structures with controlled energy absorption in the hybrid cellular automaton framework. J Mech Design 2013;135(9):091002.
[36] Duddeck F, Hunkeler S, Lozano P, Wehrle E, Zeng D. Topology optimization for crashworthiness of thin-walled structures under axial impact using hybrid cellular automata. Struct Multidiscip Optimiz 2016;54(3):415–28.